Available online at www.sciencedirect.com

SciVerse ScienceDirect

http://www.elsevier.com/locate/biombioe

Synthesis and thermo-economic design optimization of wood-gasifier-SOFC systems for small scale applications

Matteo Morandin [a,*], *François Maréchal* [b], *Stefano Giacomini* [b]

[a] *Chalmers University of Technology, Div. of Heat and Power Technology, Kemivägen 4, SE-41296 Göteborg, Sweden*
[b] *École Polytechnique Fédérale de Lausanne (EPFL), Industrial Energy System Laboratory, Station 9, CH-1015 Lausanne, Switzerland*

ARTICLE INFO

Article history:
Received 19 October 2011
Received in revised form
2 January 2013
Accepted 6 January 2013
Available online 29 January 2013

Keywords:
Biomass gasification
Pinch analysis
Thermo-economic optimization
SOFC
Synthesis

ABSTRACT

The conceptual design of a biomass integrated gasification fuel cell system for small scale applications (40 kg h^{-1} woody biomass input with 50% mass fraction water content) is discussed in this work. Two different biomass gasifiers (circulating fluidized bed and downdraft), two different reformers, a solid oxide fuel cell, a gas turbine and a heat recovery steam cycle were investigated. A two-step optimization procedure was used to perform thermo-economic design optimizations of nine system configurations generated by combining different technologies. At the master level an evolutionary algorithm is used to optimize the system intensive parameters following the minimization of the system costs and the maximization of the net power production simultaneously (two-objective). At the inner level, system mass flow rates are optimized by linear programming subject to the thermal balance and to the heat transfer feasibility constraints which were formulated by means of Pinch Analysis techniques. The degree of system internal heat recovery was studied by including the minimum temperature difference between hot and cold streams as a decision variable at the master optimization level. Optimization results are shown by means of an optimal Pareto front for each configuration. The degree of system internal heat recovery of some specific solutions is discussed by means of Pinch Analysis composite curves. The study shows that very high system efficiencies can be obtained but only at the expense of really high system costs mainly because of the high costs of the fuel cell and of the gasifier especially at the small scale level considered here. Minimum specific plant costs of the most cost-effective configuration, based on a hybrid cycle, greater than 7000 \$ kW^{-1} (2010 dollars) are found. The indirect circulating fluidized bed gasifier appears the most promising choice both in terms of cost and of system performance since it allows for better thermal integration at high temperatures and greater hydrogen yields. Autothermal reforming is a cheaper solution compared to steam reforming but does not benefit of the system internal heat recovery thus leading to comparably lower system efficiency. Steam reforming is particularly convenient when the system is pressurized and extra power can be recovered by gas expansion since a great amount of steam can be injected prior the reformer and vaporized by recovering the heat from exhaust gases.

* *Corresponding author*. Tel.: +46 (0)31 772 8536; fax: +46 (0)31 82 1928.
E-mail addresses: matteo.morandin@chalmers.se, matteo.morandin@gmail.com (M. Morandin).
0961-9534/$ – see front matter © 2013 Elsevier Ltd. All rights reserved.
http://dx.doi.org/10.1016/j.biombioe.2013.01.003

Nomenclature

ΔT	temperature difference
η	efficiency
ac	air compressor
aux	auxiliaries
AD	air drier
Arec	anode recycle
ATR	autothermal reformer
BIGFC	biomass integrated gasification fuel cell
BPgas:	by-pass gas stream to combustion
C	cost
cnd	low pressure steam header
Crec	cathode recycle
CU	cold utility
EJ	ejector
ext	medium pressure steam header
FB	FICFB (Fast internally circulating fluidized bed) gasifier
FU	fuel utilization (SOFC)
GAS	gasifier
GT	gas expander
HEN	heat exchanger network
HEX	heat exchanger
in	inlet
is	isentropic
J	current density
m	mass flow rate
min	minimum
MINLP	mixed integer non-linear programming
out	outlet
p	pressure
P	power
PC	post-combustion
Q	heat load
REF	reformer
RNK	steam cycle (Rankine)
S/B	steam to biomass ratio (FB gasifier)
S/C	steam to carbon ratio (steam reforming)
SC	stoichiometric combustion
SOFC	solid oxide fuel cell
sp	high pressure steam header
STR	steam reformer
SYS	system
T	temperature
tot	total
VK	Viking gasifier
w	weight fraction
wp	water pump
x	recycle ratio

1. Introduction

Lignocellulosic biomass is one of the most common renewable resources used for power generation. As biomass is a dispersed and limited resource, the choice of the scale and of the type of the biomass conversion system appear crucial to achieve high resource efficiencies.

A possible approach is to convert biomass in liquid or gaseous fuels that can be used in high efficiency end-use energy conversion technologies. This is possible for instance by means of thermal gasification, a thermo-chemical conversion of a typically solid feedstock that occurs at high temperatures in presence of partial oxidizing or reforming agent [1]. Biomass gasification followed by gas cleaning can lead to a high-grade syngas which can be used for power generation in gas engines, gas turbine or fuel cells such as molten-carbonate or solid oxide fuel cells. Although techno-economic aspects of such high temperature advanced energy systems have been largely investigated in the past decades [2–5], such technologies are still in a development status.

The present work focuses on the conceptual design of a biomass integrated gasification fuel cell (BIGFC) system for small scale application (fixed input of 40 kg h^{-1} of woody biomass with 50% mass fraction water content, nominal power less than 100 kW).

Experimental investigations on SOFCs fueled with biomass derived syngas have been recently carried out by different research groups [6–8]. In parallel, thermodynamic analyses have also been performed to investigate system aspects. The results of some of these studies are summarized in Table 1 (in the case more than one concept is discussed in a publication, only the data about the solutions with maximum efficiency are shown).

It is clear that the combination of fuel cell with another energy conversion technology such as gas or steam turbine allows higher performances than the concepts based on fuel cell only. On the other hand, it is also evident that different modeling approaches and assumptions are the main reasons beyond different values of efficiencies estimated in different studies. In particular, we want to stress the fact that several system concepts can be obtained with the same *basic components* (e.g. gasifier, fuel cell, gas turbine, etc.) simply by arranging differently the heat exchanger network used for system internal heat recovery [20]. The degree of system heat integration emerges as a crucial design aspect when aiming at high performances and can compete in terms of costs and technical constraints with choices related to the design of single equipment units.

Although experimental investigations are necessary to help understand the technical viability of such system concepts, very low heat integration is usually implemented in laboratory test rigs so more general approaches based on theoretical models are necessary to predict the system complexity required to reach high efficiency. Comparative analyses between technologies accounting both costs and thermodynamic performances like in Refs. [8,21,22] are necessary to understand the potential role of BIGFC systems in future energy scenarios.

We observe that the choice of the scale of the system is somewhat constrained by the size of the fuel cell system. In our case we decided to investigate the use of a planar anode-supported type of SOFC which has not yet been demonstrated in size bigger than tens of kW [23]. Conversely, gasifiers, especially of fluidized bed type, are generally economically

Table 1 – Summary of recent literature on biomass integrated gasification SOFC systems. Fixed: fixed bed gasifier; FB: Fluidized bed; GT: gas turbine (hybrid); ST: steam cycle (combined).

Reference	[9]	[10]	[11]	[12]	[13]	[14]	[15]	[16]
Scale	100 kW	10.1 MW	250 kW	170 kW	200 kW	140 kW	1 MW	30 MW
Fuel composition mass fraction dry basis								
C (%)	49.3	55.5	[17]	51.2	n.a.	51.2	40	50
H (%)	5.9	5.55		6.1	n.a.	6.1	5.35	6.12
N (%)	0.6	–		0.76	n.a.	0.76	0.62	0.55
O (%)	44	38.9		39.3	n.a.	39.3	44.5	42.5
S (%)	0.02	–		0.09	n.a.	0.09	0.15	0.06
Cl (%)	0.162	–		–	n.a.	–	–	–
Ash (%)	–	–		2.6	n.a.	2.6	9.41	0.8
Moisture (%ar)	12	10		10	n.a.	10	10	25.2
Equip. specs								
Type gasifier	Fixed	n.a.	Viking	FB	FB	FB	FB	Circ. FB [18]
Oxidizing agent	Air	Cathode air	Air	Steam	Air	Steam	Steam	Air
Gasifier temp (K)	1073	1573	–	1073	1173	1073	1223	1223
Min. gas cleaning temp. (K)	873	817	573	723	573	343	973	n.a.
TAR reformer	Yes	Yes	No	Yes	No	Yes	No	Yes
Type SOFC	Ni/GDC LSM	n.a.	Risø [19]	n.a.	Planar int. ref.	Ni/YSZ LSM/YSZ	n.a.	n.a.
SOFC outlet temp. (K)	1273	1268	1073	1173	1223	1173	1073	1223
Current density (A cm^{-2})	0.25	n.a.	0.3	0.3	n.a.	0.25	0.37	0.25
Fuel utilization (%)	85	80	85	85	n.a.	70	85	80
SOFC recirculation	Anode, cathode	n.a.	Anode, cathode	–	–	–	–	Anode, cathode
Auxiliary	Micro-GT	GT	GT (η 75%)	–	–	–	ST (η 75%)	GT (η 91%)
Turbine inlet temp. (K)	1273	1473	1173	–	–	–	–	1393
Maximum pressure (MPa)	0.7	n.a.	0.25	0.1013	0.1013	0.3	0.5	0.8
Heat exchangers	7	2	6	3	2	3	6	5
Max. eff. LHV (%)	54	42	50	34	23	36	64.4	50

interesting at a much bigger scale. Thus, when looking at the integration of biomass gasification with a fuel cell system a possible successful approach is to build a centralized gasification plant that provides syngas or SNG [24] to a large number of decentralized fuel cell systems [25–27]. In such arrangements however all the possible heat integration opportunities between the gasifier island and the decentralized fuel cell islands are lost.

In this work we followed an alternative design approach that is to adapt the gasifier size to the fuel cell scale. The results of the present analysis should help in understanding the impact in cost and efficiency of synthesis and design choices, particularly those resulting from the high heat integration opportunities. Together with experimental results conducted by some research partners on small scale BIGFC systems, the results of this study can be compared with the option consisting of one big gasifier and decentralized fuel cell system and to identify most promising system configurations.

2. Methodology

To compare different system configurations in a systematic way, the change in system topology (types of components and their connections) is addressed by introducing a system superstructure that includes all the basic components (Fig. 1), in which all the possible *basic plant configurations* can be identified by virtually enabling mutually excluding components [20].

In principle, the overall optimization problem could be programmed as an MINLP problem, whereby all the technological alternatives are evaluated at once and the optimal plant configuration is found as a result of a single optimization problem. We chose instead a different approach in which the different plant configurations were optimized separately following the maximization of the system efficiency (ratio between the total net power and input of wood chemical energy rate as in Eq. (1)) and minimization of the capital investment simultaneously (two-objective optimization). In this way the resulting Pareto fronts of the different system concepts are compared graphically and conclusions are drawn based on the position of significant system designs in the cost–performance diagrams.

$$\eta^{SYS} = \frac{P^{SYS}}{m_{WOOD} \cdot LHV_{WOOD}} \quad (1)$$

In addition we decided to discard any pre-defined HEN design and to use a methodology that evaluates heat recovery targets given the set of system hot and cold thermal streams. A pre-defined HEN is in fact optimal only for a specific set of equipment units and their design parameters and it generally constrains the system performance to lower values as soon as different equipment units and different values of their design parameters are considered. The system internal heat recovery was therefore studied by looking at the process internal heat cascade through on Pinch Analysis techniques [20,28,29]. Accordingly, the system thermal streams are separated into

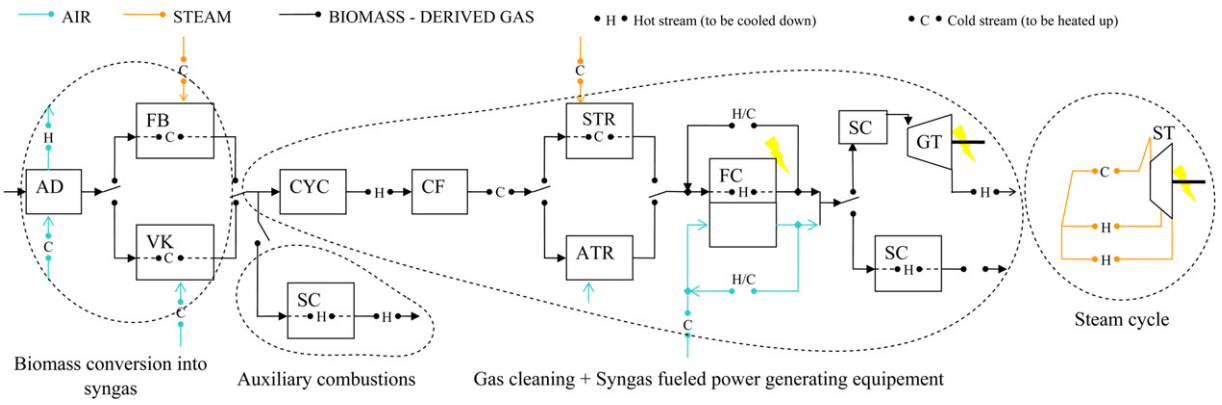

Fig. 1 – System superstructure. AD = air drier, FB = fast internally circulating fluidized bed gasifier, VK = Viking gasifier, SC = stoichiometric combustion, CYC = cyclone, CF = candle filter, STR = steam reformer, ATR = autothermal reformer, FC = fuel cell, GT = gas turbine, ST = steam turbine.

two subsets, the cold thermal streams (system heat sinks) and the hot thermal streams (system heat sources). By choosing an appropriate value of the minimum allowable temperature difference between hot and cold streams, the maximum amount of heat that can be recovered by cooling the hot streams and heating the cold streams can be estimated by an algebraic procedure (see "problem table" in Ref. [28]). This methodology allows exploring different system topologies and therefore to optimize the system design parameters independently of the way the system thermal streams are matched. In so doing, the HEN synthesis is separated from the system conceptual design and is left to be tackled as a subsequent problem which is not discussed here. To include the HEN costs in the total capital costs accounting, the HEN capital costs were estimated as a function of an average heat transfer surface and the minimum theoretical number of heat exchangers (see Euler's rule applied to HEN design in Ref. [28]).

The estimation of the maximum internal heat recovery with Pinch Analysis returns as a complementary result the process heat deficit at high temperatures (so called hot utility). As the system must be thermally self-sustaining, a constraint must be included to impose that no external hot utility is ultimately required. In practice, in our system, this corresponds to evaluate the amount of gas from the biomass gasifier that needs to be burnt in auxiliary burners to sustain the process heat requirement such as the indirect gasification, steam reforming or any other cold stream which are not sufficiently covered by the other system heat sources (e.g. the combustion of the unreacted char leaving the gasifier or the unreacted fuel leaving the fuel cell). To do this, the system was subdivided into subsystems which are highlighted with dashed lines in Fig. 1. The mass flow rates flowing through the subsystems were optimized through linear programming subject to the Pinch Analysis heat transfer constraint (no violation of the minimum temperature difference), to null hot utility demand constraint and to material balances at splitters.

A two-step optimization procedure was therefore used to tackle the overall system design optimization of each configuration following both costs and performance objectives. In so doing the intensive parameters are optimized in an outer step while the system mass flow rates (the right amount of syngas to be by-passed to the auxiliary combustion to guarantee the system thermal balance, plus the mass flow rates of other independent subsystems like the steam cycles and the cold utility) are calculated in an inner linear programming step. A more detailed description of the thermo-economic optimization problem is given in Section 3.

2.1. *System modeling*

The modeling of the various system components considered in this study was the object of recent works at the Industrial Energy Systems Laboratory at EPFL mainly in the field of biomass gasification, SNG production, and SOFC [24,30–32]. The present work aims at combining such an expertise under the light of a system analysis.

All the equipment responsible for the mechanical and thermo-chemical conversion of the material streams is shown in the system superstructure shown in Fig. 1. A short description of the modeling assumptions is given below while the reader is referred to the Supplementary material for more detail.

The system fuel input consists of 40 kg h^{-1} of woody biomass of average wood-composition (dry weight basis: C 51.11%; O 42.95%; H 5.75%; N 0.19%) and 50% moisture (a more conservative assumption compared to the previous works mentioned in Table 1). Since such a big amount of moisture in the feedstock can reduce the kinetics of the subsequent thermo-chemical reactions [33], the biomass is firstly sent through a rotary drum air-drier where the biomass moisture content is reduced in the presence of air at 473 K.

The biomass is then gasified either in a fast internally circulating fluidized bed gasifier (FB) or in a Viking gasifier. 90% carbon conversion is considered for FB gasifier. TAR production is fixed at 1 and 10 g m^{-3} (at standard condition of 298 K and 101.3 kPa) respectively for the Viking and FB gasifier according to a general assumption about TAR level of downdraft fixed bed gasifier and fluidized bed gasifier found in Ref. [34]. While the raw gas outlet temperature is treated as a decision variable for both the gasifiers, the temperature and the

conversion of biomass into volatiles in the pyrolysis stage of the Viking gasifier were fixed respectively to 873 K and 85%. A pressure drop of 5 kPa was considered in both the gasifiers.

The bigger share of the produced gas is cooled down to 773 K and sent to the hot gas cleaning section. This consists of a cyclone and a ceramic filter in which the fine particles of solids are removed. Sulfur based compounds and hydrogen chloride in syngas can also be highly detrimental for the subsequent gas upgrading equipment and the SOFC should be removed in case of high sulfur and chlorine concentration in the biomass. Although their impact in system performance is in fact negligible, they can require additional investment which was here not considered due to the absence of reliable cost data. A total pressure drop of 7 kPa was assumed for the cleaning section.

Subsequently, the gas undergoes an upgrading process either in a steam reformer or in an autothermal reformer where some heavy hydrocarbons, which may be detrimental for the SOFC, are transformed into lighter compounds. The syngas in the reformer is assumed to reach the thermodynamic equilibrium. Steam reforming indeed exploits the heat available in the process to increase the syngas hydrogen content. The obtained syngas mainly consists of methane, hydrogen, carbon monoxide, and steam. A pressure drop of 2 kPa was assumed for both the reformers.

The syngas then enters a planar anode-supported SOFC. By connecting the SOFC to an electrical load, the oxygen ions diffuse from the cathode through the electrolyte in the presence of high temperatures and produce a current while reacting with the hydrogen and carbon monoxide at the anode side. The size of the SOFC is estimated considering a parallel arrangement of stacks with 200 cells, each cell with an area of 200 cm^2 (see section 3 “planar anode supported SOFC” in the Supplementary material).

For a given fuel composition, which sets the Nernst voltage, the cell characteristics (relation between cell voltage V_{cell} and current density J) depend on cell materials and arrangement but also the excess of air λ at the cathode. A given point of such V_{cell}-J characteristic curve corresponds also to a power density and to fuel utilization FU. From the modeling point of view, the set of equations used to describe the cell characteristics can be rearranged in different way by explicitly showing any of the four variables (FU, J, V, λ) as function of remaining two (the other cell physical parameters being constant). In this work, FU was regarded as a decision variable.

In order to minimize the cost of power generation, the operating points with the highest power density should be considered. Such demanding fuel cell operation would nevertheless be detrimental in the long run so the fuel cell is preferably operated at lower current density (higher cell voltages). In this work it was chosen to fix this safety point to a cell voltage of 0.7 V. While this would not prevent in theory to investigate even higher voltages, it was decided to fix the cell voltage at its lower bound (0.7 V), all the points with even higher voltage (lower power density) being in this way discarded as they would impose even higher system costs. The corresponding cathode excess of air λ required to meet the chosen operating point results from the energy and mass balances at the fuel cell. The fuel cell characteristic is shown in the Supplementary material for a given syngas composition.

Some heat is also produced due to irreversibilities of electrochemical reactions which keeps the SOFC at high temperature while providing the energy for additional reforming of methane into hydrogen and carbon monoxide. Anode and cathode recirculation are considered and ejectors are used to overcome the 5 kPa of pressure drops along the SOFC. The remaining gas depleted at the anode is mixed with the non-recirculated portion of the cathode exhaust air and burnt in a post-combustor to provide additional heat for the system.

From the point of view of the system thermal cascade, the excess heat available at some medium or high temperature levels can be used to drive a bottoming steam cycle according to the well-known combined cycle configuration [35,36]. Various configuration of steam cycles (condensing, counter-pressure or extraction-condensing turbine) are explored throughout the optimization by means of linear programming. A fixed isentropic efficiency of 0.75 is considered for the steam expansion. Alternatively, the system can be pressurized and the SOFC exhaust gases can be burnt and expanded through a gas expander with a fixed isentropic efficiency of 0.85 thus producing additional power. Assuming such high performance appears in line with technological level of the remaining equipment especially in the case of the pressurized system, provided that high rotational speeds and multiple stages are used [37]. The resulting hybrid configuration (fuel cell plus gas turbine) has been investigated in many recently published works [38,39] and is here compared in terms of performance and costs with other system concepts.

2.2. *Applying Pinch Analysis to formulate the heat transfer feasibility as a linear constraint*

The system hot and cold thermal streams were treated as a single set of thermal streams to be integrated. As shown in Fig. 2 this set comprises:

- the air heating for wood-drying (cold stream) and the cooling of the air at the drier outlet (hot stream);
- the FB gasifier thermal demand (cold stream) and the combustion of the unreacted fixed carbon (hot stream);
- the pyrolysis thermal demand of the Viking gasifier (cold stream);
- the gas cooling of the raw gas before the particle size removal (hot stream), the gas preheating before the steam reformer or the auto-thermal reformer (cold stream), the thermal demand of the steam reforming (cold stream).
- the SOFC net thermal output (hot stream);
- the combustion of anode and cathode depleted gas (hot stream);
- the cooling of the gas turbine exhaust gas (hot stream);
- the steam production thermal demand (cold stream), the steam extraction condensation (hot stream) and the turbine end-pressure steam condensation (hot stream);
- the combustion of the by-passed raw gas (hot stream).
- the cold utility (cold stream).

For each system configuration only some of thermal streams of the above list participate to the thermal cascade, as only a subset of units of the system superstructure is considered.

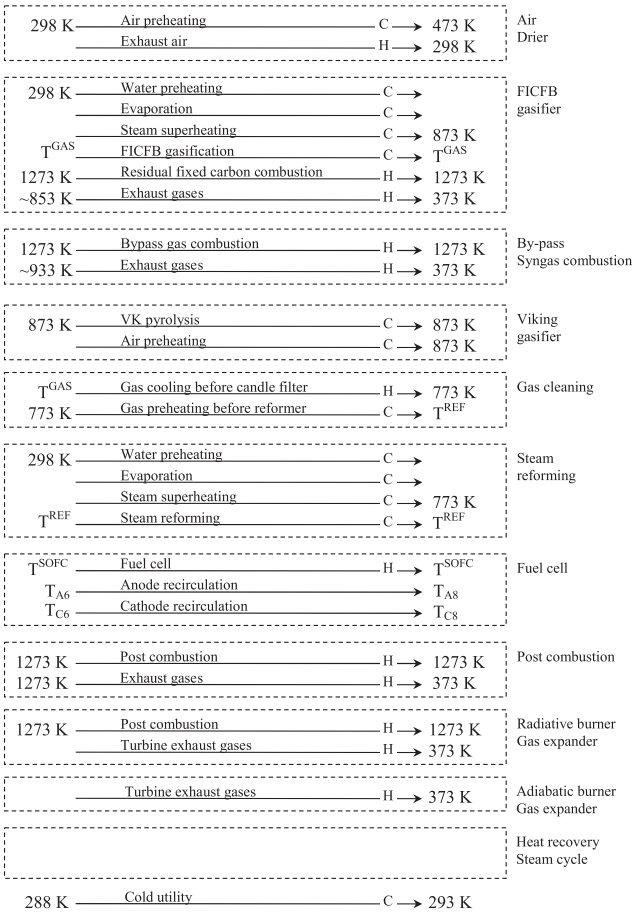

Fig. 2 – Overall set of thermal streams to be integrated (subsets of thermal streams are considered only when the related equipment unit is selected).

All the heat loads available above 1273 K are considered to be transferred through radiation and are treated as isothermal loads at 1273 K.

A variable degree of system heat integration is investigated through the optimization by including the minimum temperature difference between hot and cold thermal streams as a decision variable at the master optimization level. With this approach different amount of heat recovery between high temperature technologies such as gasifier, SOFC, combustions and reformers is explored systematically. To account for the technological constraints of high temperature heat transfer, a bigger minimum temperature difference contribution of 50 K was used for high temperature thermal sources and sinks so that, for instance, heat transfer through heat pipes is possible.

Since the HEN topology was not fixed *a priori* and since the HEN synthesis was not performed, the pressure drops in heat exchangers were not taken into account. In fact pressure drops in heat exchangers can be estimated only for a given HEN design. However, the burden of a possible HEN synthesis algorithm in the already large optimization problem would make our investigation prohibitive from the computational point view. This results in a slight overestimation of the net power and of the system efficiency.

2.3. *Investment costs*

Total grass root investment costs were evaluated through a general formulation of equipment cost proposed in reference chemical engineering literature which is based on reconciliation of commercial data about most common chemical processes equipment [40,41]. 2010 was used as the reference year for our cost estimations. The Marshall & Swift coefficient was used to update cost data from values in reference literature to 2010 basis.

The cost of the air-drier was evaluated by using the cost function of direct rotary drier with a volume of 0.1 m^3.

The cost of the FB gasifier was taken from Ref. [24]. In this reference article, the cost of the gasifier was estimated by applying general assumptions on the geometry of the gasifiers and conveyors and by applying general costing equations found in Refs. [40,41].

Conversely, the cost of the Viking gasifier was estimated according to the approach found in Ref. [24] by applying the sizing assumptions found in Ref. [30]. In particular, the gasifier was sized as a fixed bed based on the same residence time and aspect ratio of the pilot plant which sketches were found in Ref. [42] and by applying the cost function of gravity shafts. The pyrolysis stage was sized proportionally to the surface area required for the biomass input and the cost was estimated using the cost function of bucket conveyors.

The SOFC cost model in Ref. [32] was considered. Accordingly, the SOFC cost was estimated considering the specific cost of the cell, the housing cost and the cost of a pyrolysis furnace to account for the high temperature equipment.

The net system power is considered to be delivered to the electricity network through an inverter. The purchase cost of the inverter was estimated by regression of commercial data.

The HEN cost was evaluated by estimating the number of heat exchangers and the average heat transfer area as in Eq. (2) considering a fixed price of 10,500 $ per heat exchanger unit and specific price of heat transfer area of 130 $ m^{-2}.

$$10,500 \cdot N^{HEX} + 130 \cdot A^{HEN} \quad (2)$$

The number of heat exchangers N^{HEX} was calculated according to the Euler's rule [28].

The average heat transfer area A^{HEN} was estimated by dividing the total area estimated from the hot and cold composite curves by the number of heat exchangers N^{HEX} and considering a general global heat transfer coefficient of 250 W m^{-2} K^{-1} [43].

Additional costs were considered for the combined and hybrid configurations. In particular for the combined system (SOFC plus heat recovery steam cycle), the costs of heat recovery steam generators and steam condensers were included in the total cost of the heat exchanger network. The cost of steam turbine was estimated with a generalized expander cost function found in Ref. [41].

In the case of the hybrid configuration (SOFC plus gas turbine), the additional cost with respect to the case with SOFC only corresponds to that of a gas expander downstream the fuel cell, as the cost of the air blower at the cathode side and of the post-combustor is already included in the case with the SOFC only. The cost of gas expander was evaluated according to Ref. [41].

The effect of the pressure on system costs was taken into account by a multiplication factor for each equipment units and expressed as a function of the pressure. Similarly, other multiplication factors were used to estimate the final total grass root investment [41].

Although system costs were expressed in this way as a function of the system decision variables with a sufficient level of details, we have reasons to believe that the uncertainties of the cost estimates may range within a 30–40% error [44]. Still, cost data from producers of different technologies, especially in the case of pressurized system, are rare and often unreliable so the approach that we used appears the only possible for comparing the proposed system concepts in a systematic way.

3. Thermo-economic optimization problem

Thermo-economic analyses of the system configurations included in the system superstructure shown in Fig. 1 were performed separately. For each configuration, the system decision variables were optimized following maximum system efficiency η^{SYS} and minimum system costs C_{tot}^{SYS}.

A two-step optimization procedure shown in Fig. 3 was applied. In the outer optimization step an evolutionary algorithm based multi-objective optimizer [45] was used. The following system intensive parameters were considered within the bounds shown within brackets:

- the wood moisture at the outlet of the air drier $w_{H_2O}^{AD}$ (0.1:0.25);
- the steam to biomass ratio in the FB gasifier S/B (0.4:1);
- the temperature of gas at the outlet of the FB or Viking gasifier T^{GAS} (1073:1273) K;
- the reforming outlet temperature T^{REF} (973:1173) K;
- the steam to carbon ratio in the steam reformer S/C (1:5);
- the fuel cell fuel utilization FU (0.4:0.9);
- the fuel cell inlet temperature T_{in}^{SOFC} (973:1100) K;
- the fuel cell anode recirculation x_{Arec} (0.1:0.9);
- the fuel cell cathode recirculation x_{Crec} (0.1:0.9);
- the fuel cell pressure p^{SOFC} (0.2:0.6) MPa;
- the steam cycle high pressure p_{sp}^{RNK} (5:10) MPa;
- the steam cycle maximum temperature T_{sp}^{RNK} (600:800) K;
- the steam extraction pressure p_{ext}^{RNK} (0.2:2) MPa;
- the steam turbine end-temperature p_{cond}^{RNK} (0.005:1.8) MPa;
- the minimum temperature difference used to estimate the thermal cascade ΔT_{min} (10:30) K.

At each master level iteration, for a given set of values of intensive parameters, the energy and mass balances of the following three subsystems are evaluated in Belsim Vali[1]:

1. Wood drying and gasification (input: 40 kg h^{-1} of wood at $w_{H_2O} = 50\%$);
2. Raw gas auxiliary stoichiometric combustion;
3. Gas cleaning, reforming and SOFC plus gas turbine when hybrid configuration is chosen;

[1] Vali Modeller 4.4. Belsim SA, Awans (BE); 2004.

All the power loads and the temperatures and thermal loads of thermal streams of the various subsystems are then passed to the inner LP optimization which is performed using a simplex based linear programming software developed at the Industrial Energy System Laboratory. This optimization is carried out following the maximization of the system net power generation (Eq. (3)) for fixed input of 40 kg h^{-1} of wood which coincides with the maximization of system first-principle efficiency. The system net power is evaluated as the sum of the power generated by the SOFC P^{SOFC}, plus the power generated by the gas turbine P^{GT} when hybrid configuration is considered, or plus the net power generated by the steam cycle P^{RNK} when the combined configuration is considered, minus the power requirement of all the plant auxiliary devices P^{aux}. This latter term comprises the power required to run the air blower for the drier (P_{ac}^{AD}), the water pump of the steam production for the FB gasifier (P_{wp}^{FB}), the air blower for the VK gasifier P_{ac}^{VK}, the water pump for steam production for the steam-reformer P_{wp}^{STR}, the blower for the SOFC cathode air (P_{ac}^{SOFC}) and the air blower for the auxiliary stoichiometric combustion of the by-passed raw gas (P_{ac}^{SC}).

$$P^{SYS} = P^{SOFC} + P^{GT} + P^{RNK} - P^{aux} \quad (3)$$

$$P^{aux} = P_{ac}^{AD} + P_{wp}^{FB} + P_{ac}^{VK} + P_{wp}^{STR} + P_{ac}^{SOFC} + P_{ac}^{SC} \quad (4)$$

At this inner problem step the total system net power is treated as a linear function of the mass flow rates of subsystem 2 and 3 where the specific power loads appear as constant coefficients and the power required by the gasification and air-drier appears as a constant value. In addition, the optimization is subject to the mass balance at the raw gas by-pass, to the system thermal balance and to the heat transfer feasibility constraint. This latter constraint was formulated according to the Pinch Analysis. For a given set of thermal streams, the so-called Problem Table is built and the positive cumulative heat loads for each temperature level are imposed resulting in a set of linear inequality constraints.

Ultimately, the inner linear programming step is used to optimize the by-pass gas flow that is burnt in the auxiliary combustion (subsystem 2) required to thermally sustain the system. This mass flow is bound by the inequality constraints as the optimization tends to increase as much as possible the gas that is used for positive power generation. In so doing, the above constraints are handled in more effective way than in the case of a single heuristic global optimization. By including the minimum temperature difference as an upper level decision variable, we ensured therefore that all the possibly interesting process configurations are eventually explored.

When the steam cycle is also considered (combined fuel cell plus steam cycle configuration), a linear steam network model is also included at the LP level and the steam mass flow rates optimized together with the gas mass flow rate that is used for auxiliary combustion.

By doing so, we therefore assume that optimal design in the Pareto front generated at the upper level will maximize the power generated by the fuel cell and the heat recovery through a steam cycle for a given minimum temperature difference. Although we are aware that this is only an approximation as intermediate combinations of smaller fuel cells and larger

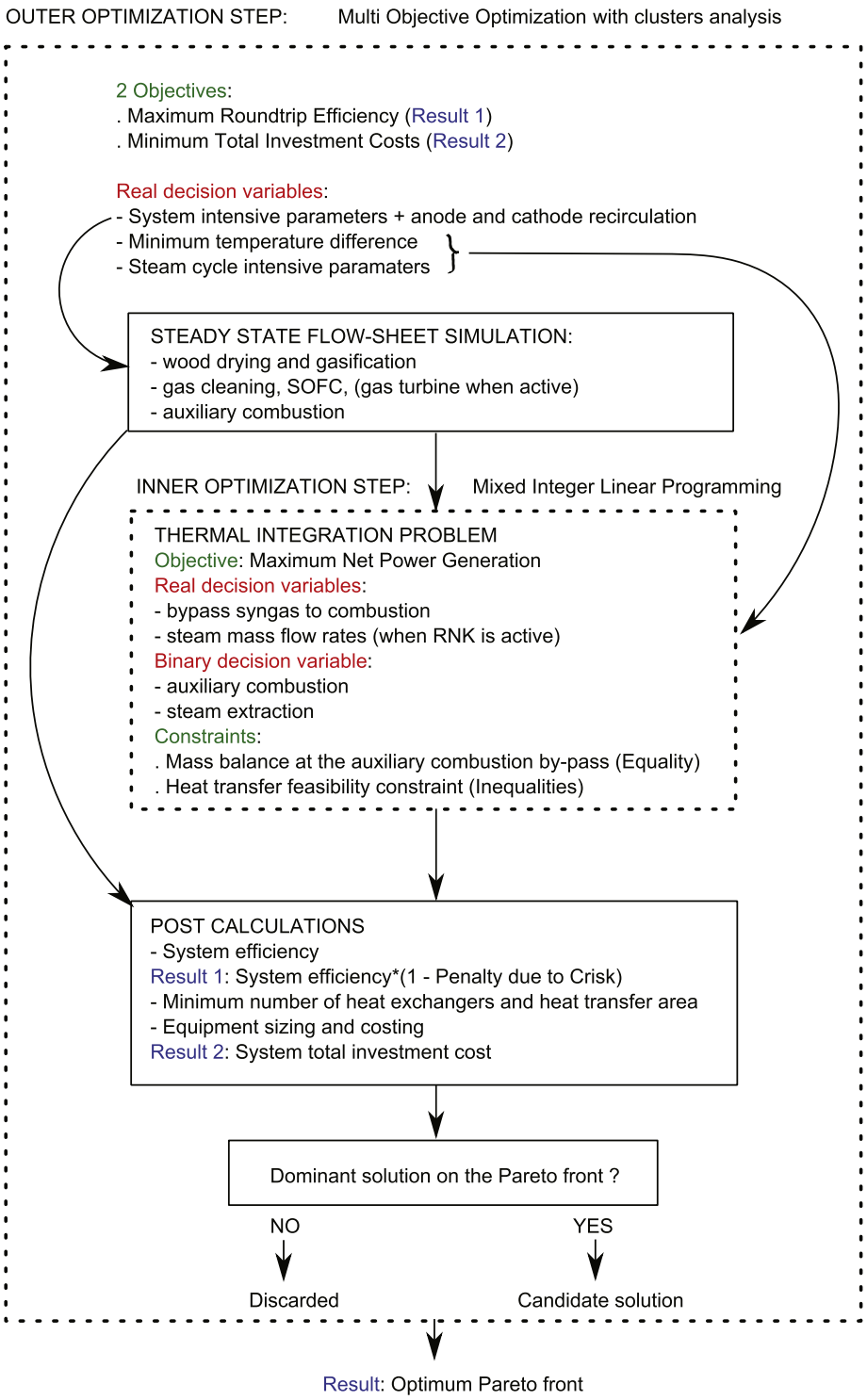

Fig. 3 – The two-step optimization procedure used for the thermo-economic analysis of each system configuration.

steam cycles using syngas combustion flue gases are not investigated, this approach was considered as being practical to generate preliminary designs and may only overestimate the cost of combined configurations at low efficiencies.

The resulting optimum mass flow rates are then used to compute the total investment cost which is the second objective of the outer optimization step. The carbon deposition risk in the reformer was included as a penalty function at the master level, being the only non-linear constraint to be handled outside the simulation model.

An evolutionary algorithm based optimizer was used to sort out the optimal values of the system intensive parameters with stopping criteria of 50,000 individuals. Optimization were carried out in a cluster of multi-core machines by using

the parallel computing capability of the Matlab[2] based calculation platform [46].

4. Results

The optimizations of nine system configurations were performed. Six system configurations are based on the FB gasifier, while the other three configurations are based on the Viking gasifier. Nine optimal Pareto fronts in the efficiency–cost diagrams were obtained. The results are discussed in three next sections where three subsets of system configurations that share the same power generating equipment (SOFC, combined cycle, hybrid cycle) are examined. Some solutions (design points) belonging to the Pareto fronts are discussed in more detail by showing the values of the decision variables and of the most significant system dependent variables (see Tables 2 and 3). The thermal integration of the most significant solutions is discussed by showing the exergy hot and cold composite curves. These diagrams give an idea of the degree of heat integration required to meet the values of the efficiency and total system costs.

4.1. *Wood gasifier, gas treatment, SOFC*

Fig. 4 shows the front of optimal solutions resulting from the thermo-economic optimizations of system configurations in which the SOFC is the power generating equipment.

The configurations with the FB gasifier completely dominate the front of the solutions of the configuration with the Viking gasifier. The choice of auto-thermal reforming instead of steam reforming contributes in general to reduce the system costs but only up to a certain level (point B at 41% system efficiency), after which the benefits of steam reforming on system thermodynamics increase and significantly higher efficiency can be obtained. In particular, steam reforming allows recovering high temperature heat into chemical energy by increasing the hydrogen content of the gas through the addition of water. The effect on the TAR conversion is in fact negligible compared to the actual impact of reforming on system efficiency, especially in the case of the downdraft gasifier.

System specific costs of the optimal solution front appear higher than 15,000 \$ kW^{-1} and, in particular, the specific costs of the VK-STR-SOFC configuration appear even higher than 25,000 \$ kW^{-1}.

Four solutions are discussed in more detail: point A and point B(STR) of the FB-STR-SOFC front, point B(ATR) of the FB-ATR-SOFC front at the same system efficiency and costs of point B(STR), and point V of the VK-STR-SOFC at the same system efficiency of point A.

The values of the decision variables at these points are reported in Table 2 while the values of other major system dependent variables are shown in Table 3. The system efficiency η^{SYS} appears strictly related to the SOFC efficiency η^{SOFC} being the SOFC the device where the chemical energy of the gas is eventually converted into electric power. For this reason, the internal (cell) fuel utilization FU is the parameter that has a direct relationship with the system efficiency and total costs. In particular, in point A, FU is close to its lower bound (0.4). However high fuel and cathode recirculation help increase the actual conversion of the fuel (actual fuel utilization). In fact, with higher values of FU, the concentration of CO, H_2, and CH_4 at the anode outlet decrease against an increase of oxidation products (CO_2 and H_2O). Due to the high recirculation, the concentrations of these species decrease also the anode inlet. Due to lower partial pressures of the reactive species the Nernst potential decrease and so does the corresponding current density J at the fixed cell voltage of 0.7 V (e.g. compare J of solution A and B(STR)). A similar effect is obtained when part of the gas in burnt in air before the gas is used in the fuel cell (e.g. in the case of the Viking gasifier as in point V or in the case of auto-thermal reforming as in point B(ATR)). The increased share of N_2 in the syngas reduces the current density. With low current densities, high system power outputs can be obtained only with great SOFC areas which increase dramatically the capital investment.

In Fig. 5, the costs of the main equipment are shown for the four solutions here examined. It is clear that the biggest difference in total costs between the configuration with the Viking gasifier and those with the FB gasifier is due to the cost of the gasifier itself. While for the FB-STR-SOFC and for the FB-ATR-SOFC, the fuel cell cost appears the biggest part of the investment, in the case of the VK-STR-SOFC configuration the Viking gasifier appears even more expensive than the fuel cell leading to total costs that are almost the double the FB-STR-SOFC configuration.

The HEN cost is another important part of the total investment. Results show that it is worth minimizing the minimum temperature difference to the lower bound (10 K) to maximize the degree of thermal integration. For all the solutions found, the heat from the SOFC, from the post-combustion (plus the combustion of the residual fixed carbon in case of the FB gasifier) is sufficient to balance the high temperature heat sinks (e.g. gasification and steam reforming).

The heat of the SOFC is removed by cooling the SOFC internally (heat load Q^{SOFC}) and by cooling the anode recycle stream (heat load Q^{SOFC}_{Arec}). Conversely, the cathode recycle stream must be heated up to high temperatures in order to preheat the charge of fresh air that provides new oxygen for the SOFC reactions.

FU and the anode and cathode recirculation are in fact the key parameters not only for the fuel cell performance but also for the system thermal balance since these parameters determine the amount of fuel to be converted into electricity and, as a complementary part, the amount of fuel that is burnt in the post-combustor.

Exergy composite curves of solutions A, B, and V are shown in Figs. 6–8 respectively.

It is interesting to notice that comparably high system efficiencies are obtained with the configuration FB-ATR-SOFC when the amount of unreacted fuel is enough to achieve the system thermal balance (a pinch point is activated at the gasifier temperature in Fig. 7). Conversely, for solution A, B(STR) (Fig. 6) and V (Fig. 8), the heat available from the fuel cell, from the char combustion, and from the post-combustor is more than enough to cover the heat demand of the cold thermal streams and no pinch point is active. The convective

[2] Matlab R2009a. The Mathworks Inc, Natick (MA); 2009.

Table 2 – Values of the objectives and decision variables of the solutions highlighted in Figs. 4, 9 and 13.

Solution	V	A (STR)	B (STR)	B (ATR)	C (ATR)	D (ATR)	D (STR)	E (ATR)	F (STR)
Objectives									
η^{SYS} (%)	34.1	34.3	41.4	41.3	46.4	57.9	58.2	56.0	68.4
C_{tot}^{SYS} (k$)	784.5	528.5	662.7	658.6	518.7	665.	665.2	399.6	506.4
Decision variables									
FU (–)	0.51	0.41	0.56	0.62	0.40	0.52	0.45	0.56	0.47
x_{Arec} (–)	0.53	0.53	0.45	0.52	0.66	0.66	0.73	0.54	0.60
x_{Crec} (–)	0.81	0.82	0.82	0.85	0.82	0.82	0.82	0.85	0.86
T^{SOFC}_{in} (K)	1084	1099	1087	1089	1090	1090	1083	1100	1100
T^{REF} (K)	992	1031	1028	973	973	973	974	974	973
S/C (–)	1.04	1.71	1.66	–	–	–	1	–	2.19
$w^{AD}_{H_2O}$ (–)	0.17	0.10	0.15	0.11	0.11	0.10	0.21	0.10	0.15
T^{GAS} (K)	1077	1085	1079	1172	1188	1165	1085	1216	1073
S/B (–)	–	0.40	0.41	0.41	0.44	0.44	0.40	0.40	0.40
p^{SOFC} (MPa)	–	–	–	–	–	–	–	–	0.60
p^{RNK}_{sp} (MPa)	–	–	–	–	7.82	9.87	9.50	–	–
T^{RNK}_{sp} (K)	–	–	–	–	795	799	790	–	–
p^{RNK}_{ext} (MPa)	–	–	–	–	–	0.34	1.13	–	–
p^{RNK}_{cond} (MPa)	–	–	–	–	0.30	0.005	0.005	–	–
ΔT_{min} (K)	11	10	11	13	11	11	10	10	10

heat of the hot thermal streams is enough to cover the steam generation thermal demand without requiring particularly large heat transfer surfaces. It also clear that the configuration FB-STR-SOFC benefits much more from the heat integration than the configurations FB-ATR-SOFC and VK-STR-SOFC. Fewer opportunities for internal heat recovery are available in these latter configurations and a big share of the heat from the SOFC and the combustion is not exploited for heating endothermic reactions or converted into electricity.

In the case of the configuration with the Viking gasifier, the increase in power output (system efficiency) can be still done by increasing the fuel utilization of the fuel cell but much less

Table 3 – Values of main system operating condition of the solutions highlighted in Figs. 4, 9 and 13.

Solution	V	A (STR)	B (STR)	B (ATR)	C (ATR)	D (ATR)	D (STR)	E (ATR)	F (STR)
SOFC fuel composition (molar fractions)									
CO_2 (–)	0.134	0.130	0.131	0.119	0.126	0.126	0.147	0.161	0.147
H_2O (–)	0.199	0.328	0.322	0.132	0.145	0.143	0.237	0.247	0.413
CO (–)	0.140	0.135	0.137	0.227	0.216	0.211	0.169	0.137	0.079
CH_4 (–)	0.002	0.001	0.001	0.017	0.023	0.023	0.033	0.056	0.024
H_2 (–)	0.292	0.405	0.409	0.381	0.378	0.364	0.414	0.320	0.336
N_2 (–)	0.232	0	0	0.125	0.111	0.133	0	0.079	0
Main system operating conditions									
p^{GAS} (MPa)	0.162	0.164	0.154	0.167	0.208	0.218	0.301	0.654	0.660
J (A cm^{-2})	0.201	0.300	0.175	0.161	0.346	0.193	0.212	0.508	0.375
Nernst (V)	0.845	0.851	0.844	0.852	0.874	0.850	0.854	0.931	0.883
η^{SOFC} (–)	0.392	0.353	0.414	0.428	0.369	0.427	0.439	0.440	0.450
T^{GT}_{in} (–)	–	–	–	–	–	–	–	1273	1693
T^{GT}_{out} (–)	–	–	–	–	–	–	–	931	1261
P^{SOFC} (kW)	34.3	35.0	41.1	41.6	36.2	40.7	44.3	42.3	40.7
P^{RNK} (kW)	–	–	–	–	9.3	15.1	11.9	–	–
P^{GT} (kW)	–	–	–	–	–	–	–	17.9	30.8
P^{aux} (kW)	4.1	4.3	4.1	4.5	3.9	3.8	4.1	9.9	10.2
P^{SYS} (kW)	30.2	30.7	37.1	37.1	41.6	51.9	52.1	50.2	61.3
Q^{GAS} (kW)	−6.2	−16.8	−17.7	−24.4	−24.9	−22.6	−17.6	−21.9	−13.4
Q^{STR} (kW)	−2.7	−14.2	−14.6	–	–	–	−12.7	–	−13.4
Q^{SOFC} (kW)	10.2	6.6	13.9	13.2	6.8	11.4	7.9	2.2	0.1
Q^{SOFC}_{Arec} (kW)	1.09	1.85	1.09	0.48	2.42	2.78	5.24	0.46	1.53
Q^{SOFC}_{Crec} (kW)	−8.28	−8.95	−9.31	−5.54	−8.5	−8.36	−8.63	−0.05	1.05
Q^{SC} (kW)	24.8	40.6	28.2	18.9	31.2	19.9	22.8	26.2	–
CU (kW)	53.1	45	39.8	51.6	45.9	36.9	31.5	38.7	12.2

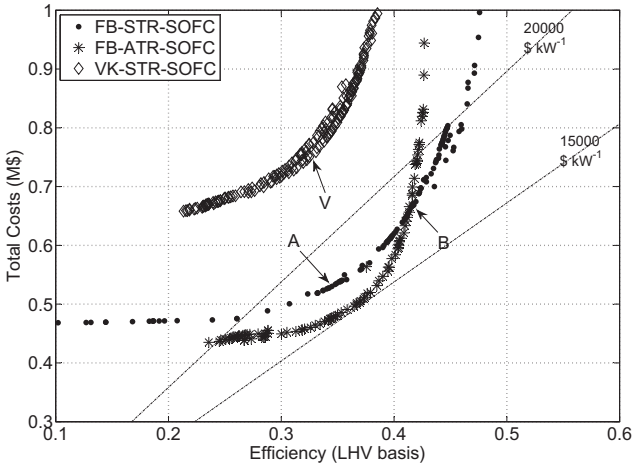

Fig. 4 – Fronts of optimal cost-efficiency design solutions with only SOFC as power generating equipment.

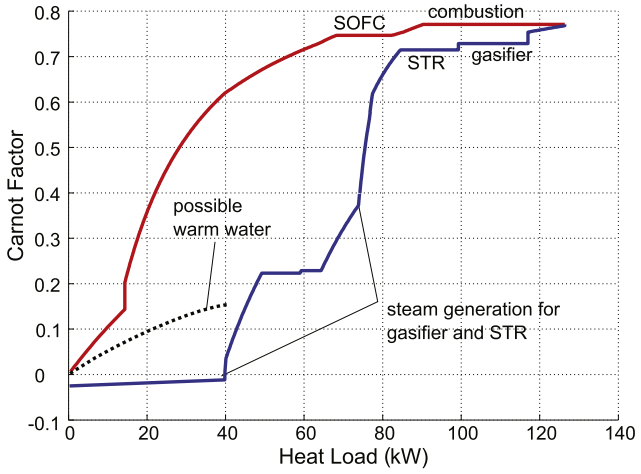

Fig. 6 – Solution B(STR): exergy hot and cold composite curves.

gain in performance can be obtained by the heat integration. This system results very SOFC-oriented and greater performances can therefore be obtained only at the expense of greater fuel cell areas.

4.2. *Wood gasifier, gas treatment, SOFC and steam cycle (combined mode)*

Fig. 9 shows the front of optimal solutions resulting from the thermo-economic optimizations of system configurations in which power is generated by the SOFC and by an additional heat recovery steam cycle (combined cycle mode).

In the same figure the Pareto fronts previously presented are also shown in the background. The addition of the Rankine cycle allows gaining in performance at lower costs. Still, specific costs results higher than 11,000 $ kW^{-1} for the configurations based on the FB gasifier and higher than 17,000 $ kW^{-1} for the configuration with the Viking gasifier. By comparing the relative distance between the VK–STR–SOFC–RNK and the FB–STR–SOFC–RNK Pareto fronts, the same pattern is found as in the previous case where the configurations with only the SOFC were compared. The cost of the Viking gasifier is the major reason for such difference. In addition, the choice of the steam reforming in place of the auto-thermal reforming allows increasing maximum performances. As already pointed out, some N_2 is injected with the air in the auto-thermal reforming to allow partial oxidation of the syngas thus reducing the amount of reactants that can be oxidized either in the SOFC or in the post-combustor.

The Pareto fronts of the system configurations in Fig. 9 appear quite irregular and consist of two competing fronts. This is particularly evident for the FB–STR–SOFC–RNK front where the crossing tails of the two subsets of solutions are shown on purpose. This is due to the activation of different pinch points corresponding to two different fronts of solutions: those with counter-pressure turbine at lower system efficiencies and those with the extraction condensing turbine at higher system efficiencies.

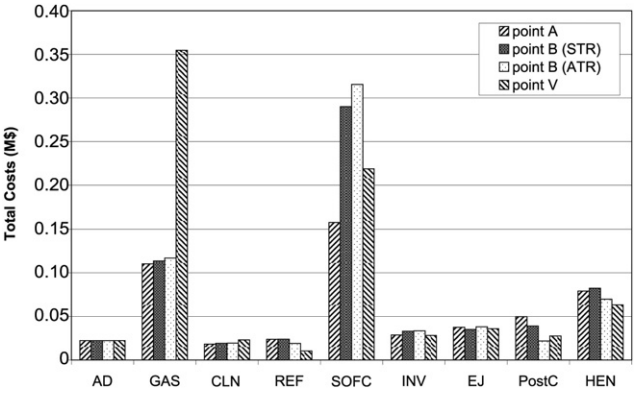

Fig. 5 – Main equipment costs for specific solutions highlighted in Fig. 4 (AD: air drier; GAS: gasifier; CLN: gas cleaning; REF: reformer; SOFC: solid oxide fuel cell; INV: inverter; EJ: ejector; PostC: post-combustion; HEN: heat exchanger network).

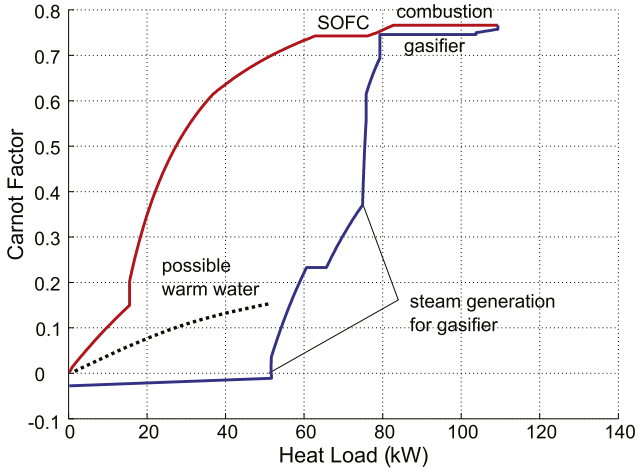

Fig. 7 – Solution B(ATR): exergy hot and cold composite curves.

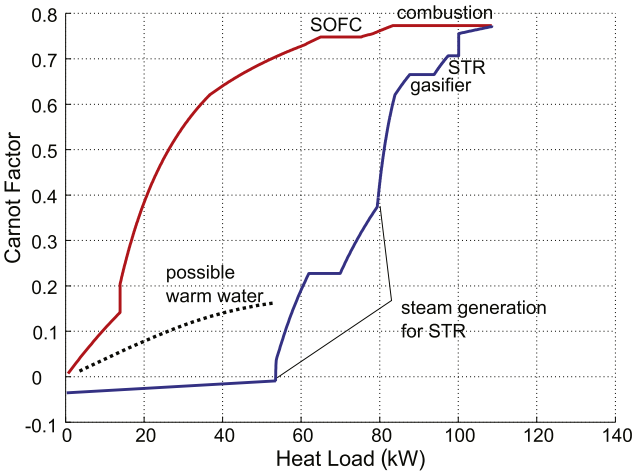

Fig. 8 – : Solution V: exergy hot and cold composite curves.

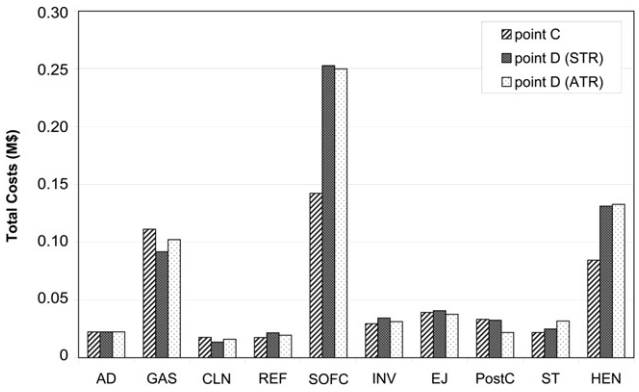

Fig. 10 – Main equipment costs for specific solutions highlighted in Fig. 9 (AD: air drier; GAS: gasifier; CLN: gas cleaning; REF: reformer; SOFC: solid oxide fuel cell; INV: inverter; EJ: ejector; PostC: post-combustion; ST: steam turbine; HEN: heat exchanger network).

Three solutions are discussed in more detail: point C and point D(ATR) of the FB–ATR–SOFC–RNK front, point D(STR) of the FB–STR–SOFC–RNK front at the same system efficiency and costs of point D(ATR). The values of decision variables and main system dependent variables are reported in Tables 2 and 3 while the main equipment costs are shown in Fig. 10.

Due to the additional power generated by the steam cycle, the system efficiency η^{SYS} is greater than the fuel cell efficiency η^{SOFC}. In particular, the steam cycle contributes for 20%–30% to the total gross power. In order to reach high values of efficiency at minimum cost it is convenient to further exploit the heat pockets of the system thermal cascade (compare the composite curves of these solutions with the previous with only the SOFC). The increase in efficiency can be done in much more cost-effective way by increasing the complexity and the mass flow rates of the heat recovery steam cycle rather than increasing the fuel cell performances.

Along the Pareto front the fuel utilization appears again the parameter with the greater influence in cost and performance (e.g. along the same FB–ATR–SOFC–STR front, compare point C and point D). Cathode recirculation is as high as in the case of the set of configurations previously analyzed (around 0.8) while anode recirculation reaches higher values (between 0.65 and 0.75). The optimal temperature of the fuel cell appears again around 1090 K. The reformer temperature is now minimized down to its lower bound (973 K). A higher anode recirculation reduces the Nernst potential and, as a consequence, the operating current density at the fixed voltage of 0.7 V decreases and so does the power density. As shown in Fig. 10, the main difference in terms of equipment costs between point C and point D(ATR) is in fact the cost of the fuel cell.

As expected, along the same Pareto front, greater performances are obtained by progressively increasing both the fuel cell and steam cycle power outputs until the cost of the fuel cell becomes too high and greater performance at low costs are obtained only by increasing the share of steam cycle power output. By comparing the values of the intensive parameters of the steam cycle of point C with point D(ATR), it is in fact possible to notice that the share of steam cycle power

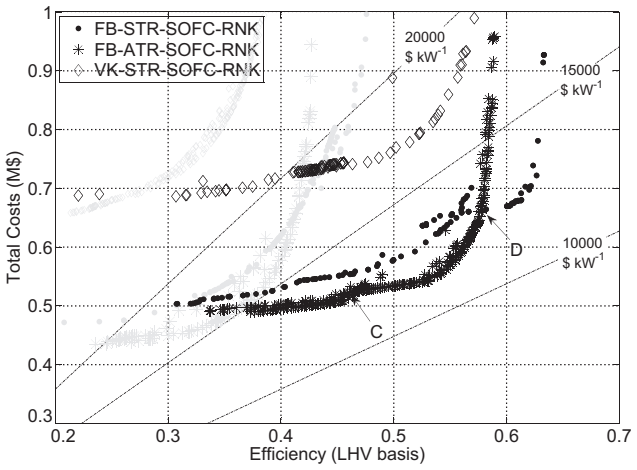

Fig. 9 – Fronts of optimal cost-efficiency design solutions based on combined SOFC and steam cycle.

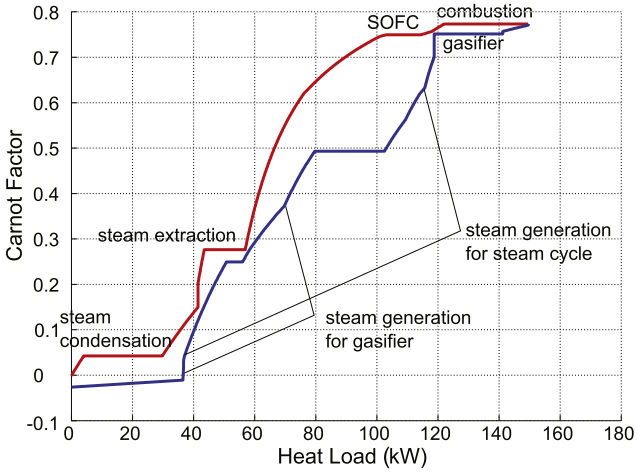

Fig. 11 – Solution D(ATR): exergy hot and cold composite curves.

P^{RNK} on the total gross power goes from 20% to 27%. Point C belongs to the subset of optimal solutions with a counter-pressure steam turbine, in this point working between 7.8 MPa and 0.3 MPa. In point D(ATR) instead, the steam cycle is of the extraction condensing turbine type, in this case working between 9.8 MPa (near the upper bound of 10 MPa) and the cold utility level (lower bound at 0.005 MPa) with a steam draw off at 0.34 MPa. This in parallel increases the complexity of the HEN for the internal heat recovery as shown by the much tighter composite curves of these solutions (Figs. 11 and 12) compared to the composite curves shown in Figs. 6–8.

By comparing Fig. 11 with Fig. 7 for instance, it is possible to notice how the increase in performance can be obtained by regularly improving the conversion of the heat pocket into net power. This can be done by regularly adjusting the steam pressures until all the pinch points are active (e.g. when 3 pinch points are active like in Fig. 11). The extraction condensing turbine has a better chance to exploit the heat pocket at lower temperatures compared to the counter-pressure steam turbine. However a big part of thermal exergy at high temperature is still lost even if the highest values of super-heating end-temperature and steam generation pressure are used.

When steam reforming is used in place of auto-thermal reforming, a greater part of heat can be recovered at high temperatures. Therefore, point D(STR) at the same system efficiency and total cost of point D(ATR) exhibits only one pinch point (compare Fig. 12 with Fig. 11). This means that there is still space for better performances by adjusting the parameters of the heat recovery steam cycle in the way that other pinch points are activated (e.g. by reducing the pressure level of the steam draw-off and by letting a greater part of steam to be expanded down to lower pressure).

4.3. *Wood gasifier, gas treatment, SOFC and gas turbine (hybrid mode)*

Fig. 13 shows the front of optimal solutions resulting from the thermo-economic optimizations of system configurations in which power is generated by means of the SOFC and of a gas

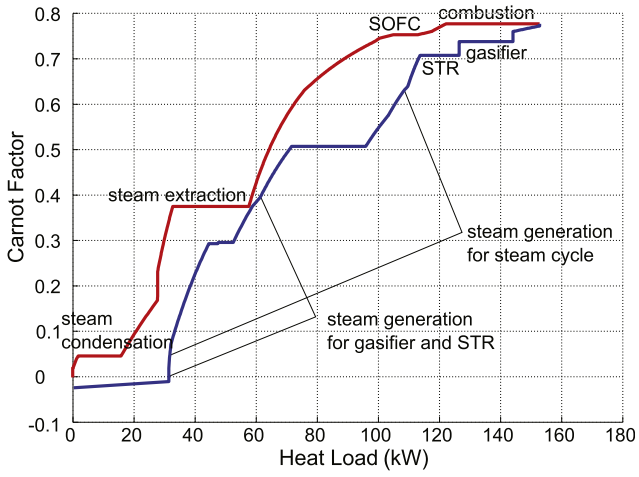

Fig. 12 – Solution D(STR): exergy hot and cold composite curves.

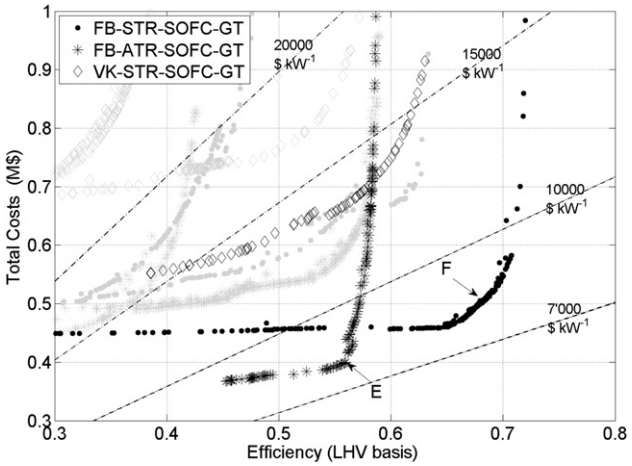

Fig. 13 – Fronts of optimal cost-efficiency design solutions based on pressurized SOFC and gas turbine.

expander while the system operates under pressurized conditions (hybrid mode). The unreacted fuel available at the SOFC outlet is burnt before the gas is expanded and two alternative designs of post-combustors are considered: radiative and adiabatic.

In the same figure the Pareto fronts of the solutions previously discussed are also shown in background. The pressurization of the system and the addition of a gas expander allow for another significant increase in performances and costs compared to the configurations in combined mode and those with only the SOFC.

Minimum values of specific costs around 8,000 \$ kW^{-1} were obtained for the configurations with the FB gasifier. The range of costs of the configuration with the Viking gasifier appear considerably higher than the other configurations, with specific costs only slightly lower than 15,000 \$ kW^{-1}. The choice of a different type of burner (adiabatic or radiative) before the gas expander has an important influence in system efficiency. In fact, the maximum system efficiencies obtained with the VK–STR–SOFC–GT configuration (around 63%) are almost 5 absolute percentage points higher than those of obtained with the FB–ATR–SOFC–GT configuration (around 58%). The difference in maximum performances is also higher when comparing the two configurations with the FB gasifier. The presence of steam reforming in place of auto-thermal reforming, in combination with adiabatic post-combustion, allows an additional boost in performance with minor increase in total plant costs. Maximum efficiencies of the FB–STR–SOFC–GT configurations are around 72%.

Two solutions belonging to these two latter configurations are discussed in more detail: point E of the FB–ATR–SOFC–GT front and point F of the FB–STR–SOFC–GT front. The main equipment costs of these two solutions are shown in Fig. 14, while the values of decision variables and main system dependent variables are shown in Tables 2 and 3.

The power recovered from the gas expansion P^{GT} represents a considerable part of the gross power output. The optimal values of fuel utilization, anode and cathode recirculation do not vary significantly compared to the previous configurations. However, higher working pressure increases

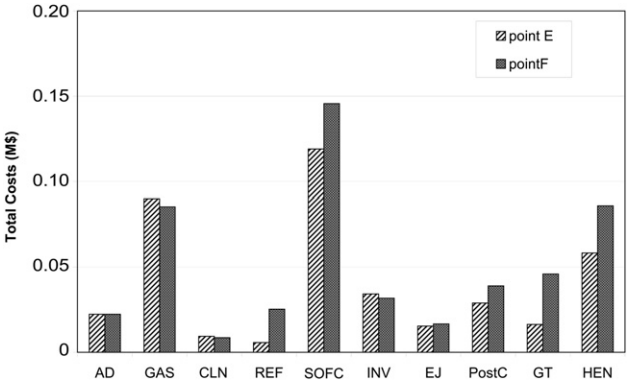

Fig. 14 – Main equipment costs for specific solutions highlighted in Fig. 13 (AD: air drier; GAS: gasifier; CLN: gas cleaning; REF: reformer; SOFC: solid oxide fuel cell; INV: inverter; EJ: ejector; PostC: post-combustion; GT: gas turbine; HEN: heat exchanger network).

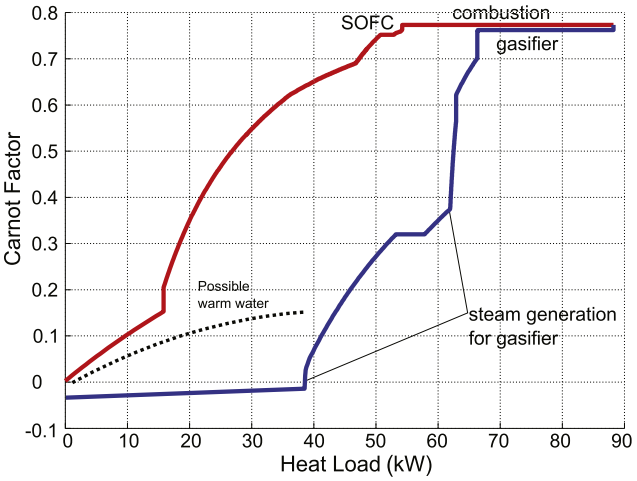

Fig. 15 – Solution E: exergy hot and cold composite curves.

the Nernst potential and the same fuel cell efficiencies can be obtained at higher current densities thus reducing the fuel cell area. Accordingly, the fuel cell cost can be kept down to almost half of the cost found in the previous sets of configurations (compare Fig. 14 with Figs. 10 and 5). Still, it is worth to point out that the increase of fuel cell costs due to pressure was modeled similarly to that of a reactor, being more reliable cost data not available, so such estimates are highly uncertain.

It is important to notice that in the case the system is pressurized, a greater benefit in performance is obtained by high cathode recirculation. This in fact reduces the amount of fresh air at the cathode thus reducing the power consumption of the air blower. In so doing the gain in net power obtained by pressurizing the system ($P^{GT} - P^{aux}$) is generally higher than the net contribution of a heat recovery steam cycles and results in a dramatic increase in performance at lower system costs compared to the case in which only the SOFC is used.

The trade-off between performance and cost of both the fuel cell and the gas expansion drives also the optimization of other decision variables. It appears particularly convenient to operate the fuel cell at the highest possible temperature (upper bound of $T_{in}^{SOFC} = 1100$ K) in order to exploit the highest enthalpy of exhaust gases. In particular, in the case of radiative burner (FB–ATR–SOFC–GT) this results in a greater portion of radiative heat available for internal heat recovery (for instance to heat up the gasification reactor through heat pipes), whereas in the case of the adiabatic burner (FB–STR–SOFC–GT) a larger power can be recovered through expansion due to higher turbine inlet temperatures. In this latter case, when the fuel utilization is low, since stoichiometric combustion is considered, the gas turbine inlet temperature T_{in}^{GT} reaches very high values that are not economically justified in commercially available micro-turbines and are almost as high as in aero-derivative gas turbines. In order to stand such high temperatures, expensive materials for turbine blades and advanced blade cooling systems are required. In this preliminary design the cost of the gas expander was roughly evaluated by extrapolating the costs of commercially available expanders used in chemical processes so most probably system costs are underestimated.

The choice of steam reforming rather than auto-thermal reforming also contributes to take more advantage of the pressurized system. In fact, steam reforming enables steam injection. Steam is mainly required to avoid carbon deposition and can also be optimized to promote higher hydrogen yields by exploiting the system internal heat recovery. In the case of the hybrid configuration, all the water that still remains at the SOFC outlet is pressurized and can be further expanded. The advantage in performance is due to the fact that the power recovered by steam expansion is a net contribution to the total power output, the pumping work being almost negligible [47,48]. For this reason, the steam amount can be maximized to increase power generation through gas expansion until a pinch point is activated. This can be better clarified by looking at the exergy composite curves of point E and point F shown in Figs. 15 and 16.

It is clear that heat pocket, still present in point E, is better exploited by steam generation in case of point F. However, in point F, steam generation does not activate a pinch point so that extra steam can be still produced by heat recovery and higher power output can be reached.

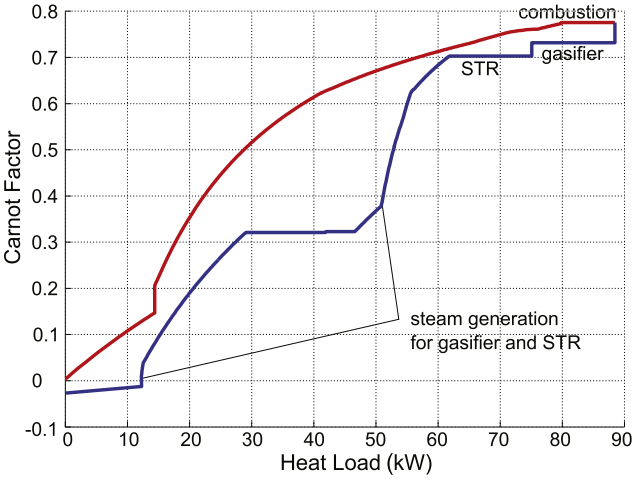

Fig. 16 – Solution F: exergy hot and cold composite curves.

5. Conclusions

The study shows that highly efficient power generation can potentially achieved with biomass gasifier SOFC systems. Based on cost estimates on state of the art technologies, such systems appear significantly more expensive than commercially available biomass based power generating systems due to the high costs of the fuel cell and of the gasifier. The competing effects of different technological alternatives were identified in this study by comparing the results of thermo-economic optimization of different configurations. The configuration with a fast internally circulating fluidized bed gasifier, steam reformer, pressurized hybrid SOFC and gas expander appear the most promising one. In this case efficiencies around 65% are reached with a total investment cost of around 450'000 $ (2010 dollars) for a nominal power of around 60 kW.

Based on this study, comparative analyses can be conducted between the proposed fully integrated BIGFC systems and systems based on a large gasifier and multiple decentralized fuel cells in which the heat integration between the gasifier and the fuel cell island is therefore not exploited. This is for instance the case in which synthetic natural gas (SNG) is produced from biomass [24] and an SNG fueled SOFC is used to produce electricity [25,26]. Assuming a 70% biomass to SNG conversion and 45% SOFC efficiency (unpressurized case) a global efficiency of 31% (biomass to electricity) is obtained for the centralized biomass gasification and distributed SOFC systems. It is reasonable to expect that economy of scale factors can be better exploited for the gas production part when a large fluidized bed gasifier is used. In addition, using methane instead of syngas can lower the SOFC costs. However, additional investment is required for the syngas methanation and CO_2 separation if an already present natural gas infrastructure must be used. Small scale integrated solutions appear therefore a highly competitive alternative if high resource efficient solutions are promoted by high electricity prices and green certificates. Such preliminary conclusions must be nevertheless substantiated with future studies in which the detailed designs of a decentralized system and of an integrated system are compared.

Acknowledgments

Stefan Diethelm and Martin Gassner at the Industrial Energy Systems Laboratory at EPFL are gratefully acknowledged for their help in system modeling. The present study was partially financed by the Swiss Competence Center for Energy and Mobility (CCEM-CH). Andrea Lazzaretto at the department of Mechanical Engineering at the University of Padova is also acknowledged for having supported Morandin's activities at the Industrial Energy System Laboratory.

Appendix A. Supplementary data

Supplementary data related to this article can be found at http://dx.doi.org/10.1016/j.biombioe.2013.01.003.

REFERENCES

[1] Higman C, Van der Burgt M. Gasification. 1st ed. Burlington (MA): Gulf Professional Publishing; 2003.
[2] Bridgwater AV. The technical and economic feasibility of biomass gasification for power generation. Fuel 1995;74(5):631–53.
[3] Kaltschmitt M, Reinhardt G, Stelzer T. Life cycle analysis of biofuels under different environmental aspects. Biomass Bioenerg 1997;12(2):121–34.
[4] Gold BA, Tillman DA. Wood cofiring evaluation at TVA power plants. Biomass Bioenerg 1996;10(2–3):71–8.
[5] Lobachyov KV, Richter HJ. An advanced integrated biomass gasification and molten fuel cell power system. Energ Convers Manage 1998;39(16–18):1931–43.
[6] Hofmann P, Schweiger A, Fryda L, Panopoulos K, Hohenwarter U, Bentzen JD, et al. High temperature electrolyte supported Ni-GDC/YSZ/LSM SOFC operation on two-stage Viking gasifier product gas. J Power Sources 2007;173(1):357–66.
[7] Nagel FP, Schildhauer TJ, Biollaz S, Stucki S. Charge, mass and heat transfer interactions in solid oxide fuel cells operated with different fuel gases – a sensitivity analysis. J Power Sources 2008;184(1):129–42.
[8] Nagel FP, Schildhauer TJ, Biollaz S. Biomass-integrated gasification fuel cell systems–part 1: definition of systems and technical analysis. Int J Hydrogen Energ 2009;34(16):6809–25.
[9] Aravind P, Woudstra T, Woudstra N, Spliethoff H. Thermodynamic evaluation of small-scale systems with biomass gasifiers, solid oxide fuel cells with Ni/GDC anodes and gas turbines. J Power Sources 2009;190(2):461–75.
[10] Athanasiou C, Coutelieris F, Vakouftsi E, Skoulou V, Antonakou E, Marnellos G, et al. From biomass to electricity through integrated gasification/SOFC system-optimization and energy balance. Int J Hydrogen Energ 2007;32(3):337–42.
[11] Bang-Møller C, Rokni M. Thermodynamic performance study of biomass gasification, solid oxide fuel cell and micro gas turbine hybrid systems. Energ Convers Manage 2010;51(11):2330–9.
[12] Fryda L, Panopoulos K, Karl J, Kakaras E. Exergetic analysis of solid oxide fuel cell and biomass gasification integration with heat pipes. Energy 2008;33(2):292–9.
[13] Omosun A, Bauen A, Brandon N, Adjiman C, Hart D. Modelling system efficiencies and costs of two biomass-fuelled SOFC systems. J Power Sources 2004;131(1):96–106.
[14] Panopoulos K, Fryda L, Karl J, Poulou S, Kakaras E. High temperature solid oxide fuel cell integrated with novel allothermal biomass gasification: part I: modelling and feasibility study. J Power Sources 2006;159(1):570–85.
[15] Sadhukhan J, Zhao Y, Shah N, Brandon NP. Performance analysis of integrated biomass gasification fuel cell (BGFC) and biomass gasification combined cycle (BGCC) systems. Chem Eng Sci 2010;65(6):1942–54.
[16] Toonssen R, Sollai S, Aravind P, Woudstra N, Verkooijen AHM. Alternative system designs of biomass gasification SOFC/GT hybrid systems. Int J Hydrogen Energ 2011;36(16):10414–25.
[17] Ahrenfeldt J, Henriksen U, Jensen TK, Gøbel B, Wiese L, Kather A, et al. Validation of a continuous combined heat and power (CHP) operation of a two-stage biomass gasifier. Energ Fuels 2006;20(6):2672–80.
[18] Ståhl K, Neergaard M, Nieminen J. Progress report: Varnamo Biomass Gasification Plant. In: Proceedings of the 1999 Gasification Technology Conference, 1999 Oct 17–20, San Francisco, California. p. 16.
[19] Linderoth S, Larsen PH, Mogensen M, Hendriksen PV, Christiansen N, Holm-Larsen H. Solid oxide fuel cell (SOFC)

development in Denmark. Mater Sci Forums 2007:1309–14. THERMEC2006.
[20] Lazzaretto A, Toffolo A. A method to separate the problem of heat transfer interactions in the synthesis of thermal systems. Energy 2008;33(2):163–70.
[21] Nagel FP, Schildhauer TJ, McCaughey N, Biollaz S. Biomass-integrated gasification fuel cell systems–part 2: economic analysis. Int J Hydrogen Energ 2009;34(16):6826–44.
[22] Arsalis A. Thermoeconomic modeling and parametric study of hybrid SOFC-gas turbine-steam turbine power plants ranging from 1.5 to 10 MWe. J Power Sources 2008;181(2):313–26.
[23] Blum L, Meulenberg WA, Nabielek H, Steinberger-Wilckens R. Worldwide SOFC technology overview and benchmark. Int J App Ceram Technol 2005;2(6):482–92.
[24] Gassner M, Maréchal F. Thermo-economic process model for thermochemical production of synthetic natural gas (SNG) from lignocellulosic biomass. Biomass Bioenerg 2009;33(11): 1587–604.
[25] Riensche E, Stimming U, Unverzagt G. Optimization of a 200 kW SOFC cogeneration power plant part I variation of process parameters. J Power Sources 1998;73(2):251–6.
[26] Costamagna P, Magistri L, Massardo A. Design and part-load performance of a hybrid system based on a solid oxide fuel cell reactor and a micro gas turbine. J Power Sources 2001; 96(2):352–68.
[27] Facchinetti E, Favrat D, Marechal F. Innovative hybrid cycle solid oxide fuel cell-inverted gas turbine with CO_2 separation. Fuel Cells 2011;11(4):565–72.
[28] Linnhoff B. User guide on process integration for the efficient use of energy. Oxford: Pergamon Press; 1982.
[29] Maréchal F, Kalitventzeff B. Targeting the minimum cost of energy requirements: a new graphical technique for evaluating the integration of utility systems. Comput Chem Eng 1996;20(S):225–30.
[30] Gassner M, Maréchal F. Thermodynamic comparison of the FICFB and Viking gasification concepts. Energy 2009;34(10): 1744–53.
[31] Maréchal F, Leuenberger S, Membrez Y, Bucheli O, Favrat D. Process flow model of solid oxide fuel cell system supplied with sewage biogas. J Power Sources 2004;131(1):127–41.
[32] Palazzi F, Autissier N, Maréchal F, Favrat D. A methodology for thermo-economic modeling and optimization of solid oxide fuel cell systems. App Therm Eng 2007;27(16):2703–12.
[33] Schuster G, Löffler G, Weigl K, Hofbauer H. Biomass steam gasification–an extensive parametric modeling study. Bioresour Technol 2001;77(1):71–9.
[34] Milne TA, Abatzoglou N, Evans RJ, Kemestrie I, Laboratory NRE. Biomass gasifier "tars": their nature, formation, and conversion. Golden (CO): National Renewable Energy Laboratory; Novemeber 1998. Report no: TP-570–25357.
[35] Kehlhofer R, Rukes B, Hannemann F, Stirnimann F. Combined-cycle gas & steam turbine power plants. Tulsa (OK) USA: Pennwell Books; 2009.
[36] Rokni M. Thermodynamic analysis of an integrated solid oxide fuel cell cycle with a rankine cycle. Energ Convers Manage 2010;51(12):2724–32.
[37] Balje OE. Turbomachines: a guide to design, selection, and theory. New York: John Wiley & Sons; 1981.
[38] Lubelli F. Internal reforming solid oxide fuel cell-gas turbine combined cycles (IRSOFC-GT): part A – cell model and cycle thermodynamic analysis. J Eng Gas Turb Power 2000;122(1): 27–35.
[39] Veyo SE, Shockling LA, Dederer JT, Gillett JE, Lundberg WL. Tubular solid oxide fuel cell/gas turbine hybrid cycle power systems: status. J Eng Gas Turb Power 2002;124(4):845–9.
[40] Ulrich GD. A guide to chemical engineering process design and economics. New York: John Wiley & Sons; 1984.
[41] Turton R, Bailie RC, Whiting WB, Shaeiwitz JA. Analysis, synthesis and design of chemical processes. 2nd ed. Upper Saddle River (NJ): Prentice Hall; 2008.
[42] Fassinou WF, Van de Steene L, Toure S, Volle G, Girard P. Pyrolysis of *Pinus pinaster* in a two-stage gasifier: influence of processing parameters and thermal cracking of tar. Fuel Process Technol 2009;90(1):75–90.
[43] Smith R. Chemical process design and integration. 2nd ed. New York: John Wiley & Sons; 2005.
[44] Feng Y, Rangaiah GP. Evaluating capital cost estimation programs. Chem Eng; 2011. p. 22–9.
[45] Molyneaux A, Leyland G, Favrat D. Environomic multi-objective optimisation of a district heating network considering centralized and decentralized heat pumps. Energy 2010;35(2):751–8.
[46] Gassner M, Maréchal F. Methodology for the optimal thermo-economic, multi-objective design of thermochemical fuel production from biomass. Comput Chem Eng 2009;33(3): 769–81.
[47] Rice IG. Steam-injected gas turbine analysis: steam rates. J Eng Gas Turb Power 1995;117:347–53.
[48] Williams RH, Larson ED. Biomass gasifier gas turbine power generating technology. Biomass Bioenerg 1996;10(2–3): 149–66.